Aging microplastics in wastewater pipeline networks and treatment processes: physicochemical characteristics and Cd adsorption

Xiaowei Li[1], Man Li[1], Qingqing Mei[1], Shiyu Liu[1], Xuan Wang[1], Huafang Xu[1], Bin Dong [2*], Xiaohu Dai[2*], John L. Zhou[3]

[1], School of Environmental and Chemical Engineering, Institute for the Conservation of Cultural Heritage, Shanghai University, Shanghai 200444, People R. China

[2], State Key Laboratory of Pollution Control and Resources Reuse, National Engineering Research Center for Urban Pollution Control, College of Environmental Science and Engineering, Tongji University, Shanghai 200092, People R. China

[3], Centre for Green Technology, University of Technology Sydney, 15 Broadway, Sydney, NSW 2007, Australia

***Correspondence Author:** lixiaowei419@shu.edu.cn (Dong B.); daixiaohu@tongji.edu.cn (Dai X.)

Abstract

Despite a wealth of information on the removal efficiency of MPs during wastewater treatment processes (WWTPs), little attention has been paid to how WWTPs may affect the MPs physicochemical characteristics. In this study, changes in physicochemical characteristics of three MPs, i.e. polyamide (PA), polyethylene (PE) and polystyrene (PS) through the wastewater pipeline, grit and biological aeration tanks were investigated. The results show that sulfidation in the pipeline (SWPN) causes a wavier MP surface, and denser holes are found on the PA surface after biological treatment in aeration tank (BTAT), but the MP surface is insignificantly affected by the mechanical abrasion in grit tank (MAGT), compared with the virgin MP. The MP zeta potentials decrease after treated by SWPN and BTAT, thus causing an increase in the MP adsorption potentials of Cd. The influence on the MP adsorption potentials is higher from BTAT than from SWPN, followed by MAGT, and all treatments lead to the change in the MP adsorption mode from monolayer to multi-layer. 2D-FTIR correlation spectroscopy demonstrates that the N-H bond in the PA plays a more important role than C-H bond in the adsorption of Cd, . The findings provide new insights into the effect of WTPs on the MP aging and physicochemical characteristics.

Keywords: microplastics; wastewater treatment plant; wastewater treatment; aging characteristics; adsorption potential

37 **Graphic Abstract**

38

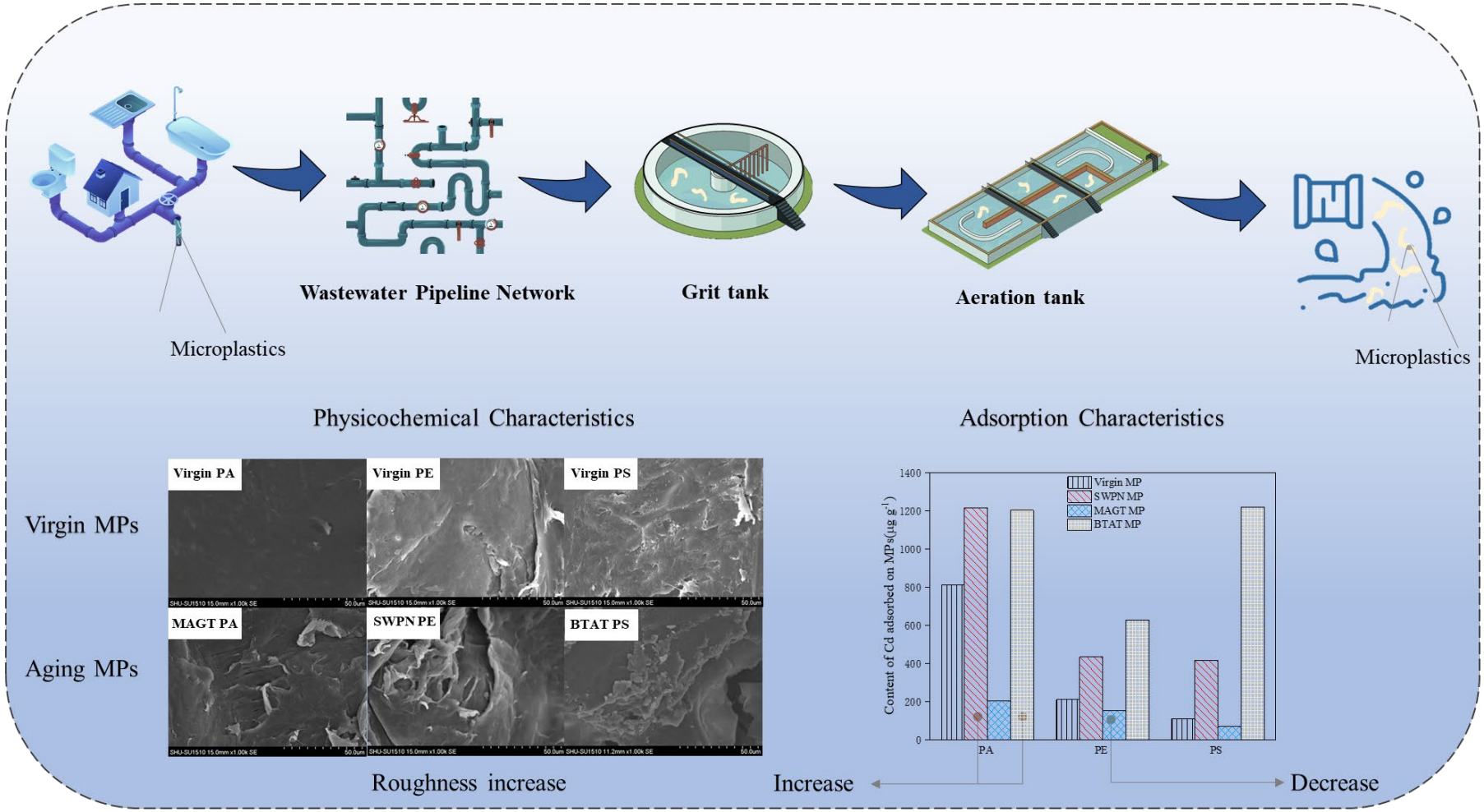

Highlights

- Changes in MP characteristics via three treatment processes were investigated
- The crack and ripples appear on the MP surface after wastewater treatment
- The SWPN and BTAT treatments cause a decrease in the MP zeta potentials
- Biological treatment has the highest effect on MP adsorption potentials of Cd
- N-H bond in PA plays a more important role than C-H bond in Cd adsorption

1. Introduction

Microplastics (MPs), often defined as plastic particles <5 mm, as emerging pollutants of environmental concern have gradually raised attention worldwide since they pose threat to aquatic species as well as human beings (Sun et al., 2019; Wang et al., 2016). MPs can be detected in all environmental systems and biota, such as rivers, lakes, oceans, sediments, marine animals and soils (Andrady 2011, Eerkes-Medrano et al. 2015, Rillig 2012, Van Cauwenberghe et al. 2013). MPs may carry organic pollutants as well as heavy metal compounds and transfer them into living organisms, which could have serious toxic effects (Li et al. 2019b). The persistent organic pollutants (POPs) adsorbed to plastics can reach up to 1 million times higher concentrations than ambient and these compounds can be further desorbed inside organisms, exasperating POPs bioaccumulation at higher trophic levels (Browne et al. 2013, Sun et al. 2019, Wang et al. 2018).

Field investigations showed that the MPs in the natural environment are weathered by environmental factors like wind, sunlight, mechanical abrasion, chemical oxidation and biological degradation in natural environments (Liu et al. 2019, Song et al. 2017, Ter Halle et al. 2016), and the altered (aged) MPs have greater adsorption of pollutants than virgin (untreated) MPs (Holmes et al. 2014, Turner and Holmes 2015, Wijesekara et al. 2018, Zhang et al. 2018). Song et al. (2017) reported that the combination of UV exposure duration and mechanical abrasion leads to the fragmentation of MPs into undetectable submicron particles. Liu et al. (2019) found that advanced oxidation

processes such as heat-activated $K_2S_2O_8$ and Fenton treatments are able to accelerate the MP aging reactions. Iniguez et al. (2018) revealed a clear loss of elasticity and an increase in the rigidity of four types of plastics after UV irradiation.

In contrast to the natural environments, wastewater treatment plant (WWTP) as a reinforced artificial treatment system might produce similar and even more serious effects on the physiochemical characteristics of MPs (Narancic et al. 2018). Until now, WWTPs are focal points in concentrating large amounts of MPs from urban sources (Freeman et al. 2020). The removal efficiency of MPs after physical and biological progress has been reported in a large number of literature (Blair et al. 2019, Carr et al. 2016, Dubaish and Liebezeit 2013, Lares et al. 2018, Talvitie et al. 2017). Few studies have paid attention to the aging behavior and physicochemical changes (e.g. adsorption potentials) of the MPs through the WWTPs (Kelkar et al. 2019). In fact, the MPs derived from the personal care and cosmetic products and washing wastewater have gone through a complex wastewater pipeline before entering the WWTP. There is usually an anaerobic environment in the pipeline network and anaerobic microbial processes are responsible for the formation of reductive compounds such as hydrogen sulfide (H_2S). This hypothesis is that the pristine characteristics of the MPs in wastewater are changed under the chemical effects of the reductive groups.

It is well known that the general processes of wastewater treatment include primary and secondary treatments. Some researchers reported that the MPs after wastewater treatment have the distinctive characteristics compared to the primitive

MPs. The processes of mixing, pumping or bubbling the wastewater in the "grit and grease" removal stage might bring the mechanical abrasion to the MPs (Li et al. 2019b). The use of treatment processes involving materials harder than MPs such as rapid sand filtration (RSF) can induce the fragmentation of MPs (Enfrin et al. 2019). The fragmentation of MPs into NPs by WWTPs increased the number of NPs/MPs in water by one order of magnitude (Enfrin et al. 2019). Meanwhile, enormous amounts of microorganisms in the activated sludge may cause biological degradation of the MPs, and then change their physicochemical properties in the aeration tank. Zubris and Richards (2005) found that the MPs in the sewage sludge have a high degree of wear or erosion and become fragile compared to the industrially produced nascent MPs. Mahon et al. (2017) implied that anaerobic digestion process may reduce the MP abundances due to the microbial breakdown polymers through the activity of exoenzymes. In addition, high content of organic matter (e.g. humic acid) in wastewater might cause an change in the structures of MPs (Chen et al. 2018). Li et al. (2019a) reported that the adsorption potential of sludge-based MPs is much higher than that of the virgin MPs. The results imply that the wastewater treatment processes can exert a significant influence on the MP physicochemical characteristics and adsorption potentials. However, the specific effect of various WWTPs on the MP properties have not yet been investigated in detail under the controlled conditions.

In this study, three potential effects on MP physicochemical characteristics were simulated during the processes that the MPs enter into and then pass through the

WWTPs, i.e. sulfidation in wastewater pipeline network (SWPN), mechanical abrasion in grit tank (MAGT) and biological treatment in aeration tank (BTAT). Then, the effects were evaluated using various techniques, such as scanning electron microscopy (SEM), Fourier transform infrared spectroscopy (FTIR), element analysis, zeta potential, adsorption potentials, and 2D FTIR correlation spectroscopy (2D- FTIR COS). The study can provide a theoretical support to understand environmental behavior and risk of wastewater-based MPs before entering the natural environment in terms of the MP aging characteristics in the WWTPs.

2. Materials and methods

2.1 Materials and reagents

Virgin MPs, i.e. polyamide (PA), polyethylene (PE) and polystyrene (PS) ranging from 150 to 300 μm were purchased from the Micro Powders, Inc., Shanghai, China. Cadmium chloride ($CdCl_2 \cdot 2.5H_2O$) was 99.0% pure and obtained from the Sinopharm Group Co. Ltd, Shanghai, China. Metal stock solutions of 1000 mg L^{-1} were prepared using deionized water. Standard metal solution was purchased from the Aladdin Industrial Corporation, Shanghai, China.

2.2 Simulating the effect of wastewater pipeline network and treatment processes

Sulfidation in wastewater pipeline network (SWPN). The SWPN effect on the MPs was investigated according to the literature (Kent et al. 2014). Briefly, the ACS grade sodium sulfide nonahydrate (Aladdin reagent) was dissolved in deionized water.

5 mmol L^{-1} sodium bicarbonate buffer was added to the sulfide solution to raise the pH value to 8.6 or higher to limit the effect of H_2S volatilization. All solutions were stored at room temperature (~22 ºC) and placed in the dark. In this experiment, 0.1 g of each MP was weighed into a 30 mL glass tube and immersed in 20 mL of 15 mmol L^{-1} Na_2S solution for 2 days, and then collected for the following analysis. Each treatment was carried out in triplicate.

Mechanical abrasion in grit tank (MAGT). SiO_2 was used as a representative grit. Both 0.1 g each MP and 0.8 g SiO_2 were added to a glass tube at a mass ratio of 1:8, and 20 mL of the configured domestic sewage was added. The glass tubes were flipped and stirred for 24 h. After that, the MPs were extracted for the following analysis. Each treatment was carried out in triplicate.

Biological treatment in aeration tank (BTAT). The simulated aeration tank was performed in a sequencing batch reactor (SBR) reactor. The reactor body was made of plexiglass with an effective volume of 6 L, as shown in Figure S1 of Supporting Information (SI). Injection and discharge of the wastewater were carried out by a peristaltic pump. The reactor temperature was kept at 25±1 ºC. The aeration pump was used for aeration, so that the dissolved oxygen of the system was held at 2-6 mg L^{-1}. The artificial sewage was prepared according to the Table S1 (SI). The SBR preparation and sludge domestication were shown in the SI.

1 g of each MP was added to a 2 L of conical flask with the 300 mL domesticated sludge and 700 mL artificial sewage. A running cycle of the SBR flask was 8 h, in which

water inflow was carried out for 1 h, aeration for 4 h, settlement for 1 h, drainage for 1 h, and idle for 1 h. The experiment was continuously operated for 14 d. After that, the MPs were extracted for the following analysis, and the activated sludge were collected for the microbial community analysis. Each treatment was carried out in triplicate.

2.3 MP extraction and analysis

The MP extraction was conducted according to the density separation method reported in our previous work (Li et al. 2018b). MP morphology was measured using scanning electron microscopy (SEM, Hitachi SU-1500, Hitachi High Technologies Corp., Tokyo, Japan). FTIR spectra of the MPs were determined with a FTIR spectrometer (Nicoq 380 MX, Thermo Fisher Scientific, MA, USA). Elemental analysis of the MPs for C, H, N and S was conducted using a macro elemental analyzer (Vario Micro cube, Germany). Oxygen content was determined by difference: O%=100-(C+H+N+S) %. The Zeta potential of MPs was measured by Zetasizer (Malvern Instru, Ltd), before the particle suspensions were ultra-sonicated overnight.

2.4 Batch adsorption experiments

The MP adsorption test was carried out according to the methods described in our previous work (Li et al. 2019a). Cd was used to estimate the changes in adsorption potentials of the MPs for heavy metal pollutants after different treatment stages. The adsorption was conducted in centrifuge tubes, each of which contained 0.05 g MP particles and 5 mL metal solution of 10 mg L^{-1} Cd. All metal solutions were prepared by diluting stock solutions with deionized water and adjusting the pH value with 0.1

mol L^{-1} HCl and 0.1 mol L^{-1} NaOH. The tubes were placed on an end-over-end shaker at 30 rpm at room temperature for 24 h. The control group was made in the same metal solution using the same procedure but without MP particles. Each test including the control was run in triplicate.

To further investigate adsorption isotherm of the MPs to Cd, the Cd concentrations were set to 1, 2, 3, 4, 5, 10, 20 and 40 mg L^{-1} as required, respectively. After 24 h of sorption, the MP particles were extracted, and the solutions were filtered using 0.45 μm membrane filter. The metal concentrations in the filtrates were measured using inductively coupled plasma optical emission spectrometer (ICP-OES), and the metal contents adsorbed on the MPs were calculated by determining the difference between the control and sample filtrate. Detailed description of the ICP-OES analysis is shown in the SI.

2.5 2D-FTIR COSanalysis of MPs Cd interactions

The MP particles that adsorbed different Cd concentration were dried for the 2D FTIR COS analysis, to further reveal the mechanism that these treatments affected the Cd adsorption on MPs to. The FTIR spectra were normalized by summing the absorbance from 4000–400 cm^{-1} and multiplying by 1000 (Li et al. 2015a, Li et al. 2014). Subsequently, the normalized data set were transformed into a new spectral matrix using principal component analysis (PCA) in Matlab R2012b (The Mathworks, Natick, USA) to reduce the level of noise (Babamoradi 2013), and then 2D FTIR COS maps were conducted using 2D Shige software (Kwansei Gakuin University, Japan)

and re-plotted by Origin 9.0 software (OriginLab Corp., Northampton, MA, USA) .

2.6 Microbial community analysis of activated sludge in aeration tank

Microbial community genomic DNA was extracted from the activated sludge samples using the E.Z.N.A.® soil DNA Kit (Omega Bio-tek, Norcross, GA, U.S.) according to manufacturer's instructions. Gene amplicons (16S rRNA gene) were carried out using PCR with primers 27F and 519R. Each primer was pre-pended with a 8-base barcode sequence and a unique barcode was applied for each sample (Li et al. 2015b). Purified amplicons were pooled in equimolar and paired-end sequenced on an Illumina MiSeq PE300 platform/NovaSeq PE250 platform (Illumina, San Diego, USA) according to the standard protocols by Majorbio Bio-Pharm Technology Co. Ltd. (Shanghai, China). Sequencing data were demultiplexed, quality-filtered on Trimmomatic, and merged according to the criteria. The quality filtered sequences were clustered into operational taxonomic units (OTUs) at 97% thresholds (Edgar 2013). Taxonomy of each 16S rRNA gene sequence was analyzed by RDP Classifier against the Silva 16S rRNA database with a confidence threshold of 70%. Finally, microbial community composition was run on the free online platform of the Major bio I-Sanger Cloud Platform (Shanghai, China).

3. Results and discussion

3.1 Changes in MP physicochemical characteristics

3.1.1 Microscopic features of MPs

As shown in Fig. 1, the cracks and pores are found on the surfaces of the PE and PS treated by SWPN, in comparison to virgin MPs, implying that the chemical treatment generated in the wastewater pipeline has an impact on the MPs, consistent with previous studies (Liu et al. 2019, Wu et al. 2020). Liu et al. (2019) and Wu et al. (2020) reported that the cracks and pits are gradually generated on the surfaces of MP in the heat-activated $K_2S_2O_8$ system. The surface of PS after BTAT becomes rougher and tends to be fragmented (Fig. 1). It indicates that the MPs are susceptible to biological erosion during biological aeration progress, possibly due to the hydrolysis and oxidation in the activated sludge system where a large number of bacteria live (Mahon et al. 2017, Rom et al. 2017). Narancic et al. (2018) demonstrated that strong microbial activity under artificial biological systems may cause MP oxidation or degradation. Compared with other treatment, MAGT causes hardly any change in the micrographs of the MP surface, indicating that it has little effect on the surface morphology of the MPs. Studies showed that the MPs are rubbed due to the shearing forces, attributed to mechanical mixing during the “gravel and grease” removal stages (Li et al. 2019a). Song et al. (2017) showed that fragmentation of MPs occurs after prolonged friction in the presence of silica sand (Song et al. 2017). In this study, the exposure time between MPs and inorganic particles was short (only 24 h), and thus no detectable change is found in the MPs.

PE spectra display the peaks at around 2916, 2849, 1471, and 718 cm^{-1} (Cooper and Corcoran 2010). The absorption peaks of PS are observed at 3083, 3061, 3024,

2923 and 2849 cm^{-1}, due to the C-H vibration of aromatic rings (Mao et al. 2020). The PA spectra possess characteristic absorption peaks of amide I band at about 1638 cm^{-1}, amide II band at about 1542 cm^{-1}, amine group at about 3300 cm^{-1}, and methylene at 3070, 2938, and 2867 cm^{-1}(Tang et al. 2009). As shown in Figure S2 (SI), FTIR spectra of the MPs after SWPN and MAGT show no significant difference in the surface functional groups from the virgin MPs, while minor changes in peak intensity of the MPs after BTAT are observed, indicating that biological treatment has higher impact on MP surface functional composition, than the other two treatments. In the activated sludge systems, the MPs come into contact with the inorganic particles and organic matter, as well as the microorganisms (Fred-Ahmadu et al. 2020). The colonization of these microorganisms with different sizes and types form the biofilms on the surface of MPs (Fu et al. 2019, Zhang et al. 2020), thus modifying the surface functional groups of the MPs (Rummel et al. 2017).

3.1.2 Elemental analysis

Compared with the corresponding virgin MPs, C, H and N contents of the treated MPs decrease, while the O content and O/C ratios increase (Table 1), showing that the treatment processes cause an increase in oxidation degree of the MPs. Compared with the SWPN and MAGT, C and H contents of the MPs after BTAT increase more drastically, implying that biological treatment has more considerable effect on the MP elemental composition, in accordance with the FTIR results. The possible reason is that the presence of some plastic-degrading bacteria on the surface of MPs causes their

256 chain scission and oxidation, and thus a decrease in the C and H contents (De Tender
257 et al. 2017). During BTAT, the changes in C and O contents of the PS are higher than
258 that of PA and PE, implying that the PS might be more easily aged than the PA and PE,
259 corresponding to the SEM results. In contrast to the secondary carbon in the PE, the
260 carbon atom bonded to the benzene ring in the PS is more susceptible to erosion,
261 resulting in rapider oxidation of PS (Gewert et al. 2015). In addition, Fig. 2 shows
262 microbial community composition of the activated sludge tank mixed with the three
263 MPs at genus level. The most abundant microorganism is *Saccharibacteria* for both of
264 the PA and PE, but *Flavobacterium* for the PS, which may supply an additional
265 explanation for the result that the biological treatment generates higher impact on the
266 PS, compared with the other two MPs.

267 **3.1.3 Surface zeta potentials**

268 Zeta potentials are associated with the adsorption potentials of chemicals on the
269 MP surface controlled by electrostatic interactions (Guo et al. 2018). As shown in Table
270 2, zeta potential of the virgin PA is 0.55±0.01 mV. After SWPN and BTAT, zeta potential
271 of the PA drops to -0.16±0.24 mV and -0.57±0.52 mV, respectively, indicating that their
272 surface negative charges increase. A decrease in surface charge of the PA after SWPN
273 might be resulted from the combination of S^{2-} and N-H. Previous literature reported that
274 most hydrophobic MPs in water enhance the adsorption of hydroxide ions, thus
275 negatively charging the microparticle surface (Fotopoulou and Karapanagioti 2012,
276 Tampio et al. 2016). A decrease in surface charge of the PA after BTAT might be resulted

277 from the attachment of organic matter in the activate sludge. The humus in the sludge
278 is usually negatively charged, and easy to attach to the MPs, resulting in an increase in
279 negative charge on the surface of PA after BTAT (Li et al. 2018a, Lu et al. 2018). Initial
280 colonization of PA by microorganisms occurs within minutes to hours (McGivney et al.
281 2020, Zettler et al. 2013), also resulting in an increase in the negative charge on the
282 surface of MPs (Rummel et al. 2017, Tribedi and Sil 2013, Zettler et al. 2013). In
283 addition, zeta potential of the PE slightly increases after SWPN, and there is no obvious
284 change in other treatments. The results therefore implied that different MPs may have
285 different response to the chemical treatment in term of zeta potential due to their
286 different monomeric composition, which deserves to be further investigated.

287 **3.2 Changes in MP adsorption characteristics**

288 **3.2.1 Adsorption potential of MPs for Cd**

289 As shown in Fig. 3, compared with the virgin MPs, adsorption potential of the
290 MPs for Cd decreases after MAGT, but increases after SWPN and BTAT. In aquatic
291 environments, the MPs show electrostatic interaction toward organic and inorganic
292 cations (Guo et al. 2018, Holmes et al. 2012, Xu et al. 2018). It is reported that the
293 adsorption of metal by MPs is mainly resulted from the electrostatic interactions (Zou
294 et al. 2020). SWPN and BTAT may cause an increase in the negative charges on MP
295 surface, which potentially enhance the role of electrostatic interactions in sorption
296 process. Such results of a decrease in zeta potentials of the PA after SWPN and BTAT
297 provide an evidence supporting the increase in the adsorption potentials.

298 Adsorption potential of the MPs treated by the processes presents a decreasing
299 order as following: BTAT > SWPN > MAGT. The result shows that the biological
300 treatment causes the highest enhancement of the MP adsorption potentials, in
301 accordance to the FTIR and elemental results. In biological aeration tanks, due to the
302 large specific surface area of MPs, biofilms are easily formed on the surface (Kaiser et
303 al. 2017, Rummel et al. 2017). Biofilm can affect the sorption behavior of MPs by
304 modifying their physical properties, including the decreased surface hydrophobicity
305 and increased heterogeneity (Johansen et al. 2019, Johansen et al. 2018, Rummel et al.
306 2017). Johansen et al. (2019) reported that biofilm can enhance the adsorption of strong
307 and weak cations onto the MPs. Holmes et al. (2012) revealed that the sorption
308 capacities of metals on weathered plastics are enriched 1.5-25 times higher than virgin
309 MPs due to the adhesion of biofilms and precipitates, consistent with our results that
310 adsorption potential of the three MPs after the biological treatment increases by 1.6-11
311 times.

312 After SWPN, the adsorption capacities of the PA, PE and PS increase by 1.6, 2
313 and 3 times, respectively, compared with the corresponding virginal MPs (Fig. 3).
314 Similarly, the adsorption capacities of the PA, PE and PS increase by 1.6, 3 and 11 times
315 after BTAT, respectively. The results show that the effect of the treatment processes on
316 PS is higher than PE, followed by PA. Higher amount of Cd adsorbed on PS in contrast
317 to PE implies that the glassy PS are possibly more susceptibly aged than rubbery PE.
318 Every other carbon atom in the PS main chain that is bonded to the benzene ring is

more susceptible to chemical attack than the secondary carbon in PE, possibly resulting in more aging of PS (Liu et al. 2019), and thus enhancing its ability to adsorb pollutants. Compared with PE and PS, increase in the PA adsorption potential after the treatment may be resulted from higher Cd adsorption by virgin PA.

3.2.2 Adsorption isotherms

To further clarify the adsorption characteristics, the Freundlich and Langmuir isotherm models were used to fit Cd adsorption data on MPs (Guo et al. 2020). The adsorption isotherm models can be described by Equations (1) and (2), respectively.

$$\frac{C_e}{q_e} = \frac{1}{k_L q_{\max}} + \frac{C_e}{q_{\max}} \quad (1)$$

$$\ln q_e = \ln k_F + \frac{1}{n} \ln C_e \quad (2)$$

In which C_e (mg L^{-1}) is the Cd concentration remaining in the solution at equilibrium, q_e (μg g^{-1}) is the amount of Cd adsorbed per mass unit of adsorbent at equilibrium, q_{max} (μg g^{-1}) is the maximum adsorption capacity, k_L (L mg^{-1}) is the Langmuir binding constant, k_F (mg^{1-n} L^n g^{-1}) and n are the Freundlich constants related to the adsorption capacity and the adsorption intensity, respectively.

Fitting results of the isothermal adsorption of the Freundlich and Langmuir models are shown in Fig. 4. The isotherms of virgin PA, PE and PS fit the Langmuir model well, implying that the adsorption is monolayer (Table 3). The Langmuir model assumes that the surface of the adsorbent is absolutely uniform with monolayer adsorption of only one molecule per adsorption site (Foo and Hameed 2010). However, adsorption isotherms of the PE and PS after SWPN, the PA after MAGT, and the PA

and PS after BTAT fit the Freundlich model well. The Freundlich isotherm is based on the assumption regarding surface heterogeneity and can be used to model multi-layer adsorption (Sintim and Flury 2017, Yang 1998). These results indicate that the treatments cause the change in adsorption mode of the MPs for Cd pollutants from the monolayer to the multi-layer. The possible reason is that the embrittlement and fragmentation of aged MPs after the treatment increase the adsorption sites and lead to the change in the MP adsorption behavior.

3.2.3 2D-FTIR COS maps

The 2D-FTIR COS was carried out to further understand the role of functional groups of the ageing MP surfaces in the Cd adsorption. Significant spectral variations are found in the ranges of 700-1700 cm^{-1}.

As shown in Fig. 5, three major auto-peaks are found in all the synchronous map of the aged PA by the three treatment processes. The intensities at 1638 cm^{-1} and 1542 cm^{-1} are higher than that at 1470 cm^{-1}, implying that the N-H functional group plays a greater role in the aging PA adsorption to Cd, compared with C-H functional groups. An asynchronous map is about diagonal antisymmetry, and thus there are only cross-peaks (Mao et al. 2020). Based on Noda's rules (Jin et al. 2018), asynchronous correlation spectroscopy can reveal the change order of the chemical bonds in the adsorption of the aging MPs to Cd. As shown in Fig. 5a and 5b, the cross-peak at 1638,1470 cm^{-1} for the SWPN and MAGT PA is positively correlated, suggesting that the adsorption of N-H functional groups to Cd was faster than that of C-H functional

groups. However, the cross-peak at 1638,1470 cm^{-1} for the BTAT PA shows the negative correlation, implying that the adsorption of C-H functional groups was faster than that of N-H functional groups, which is the opposite of the results of the SWPN and MAGT PA. The possible reason is that the attachment of organic matter and microorganism on the PA surface during BTAT causes the enhancement of the adsorption of C-H functional group to Cd, and thus promotes an increase in the adsorption potential. The results complement and confirm the findings from FTIR spectra that biological treatment has the greatest effect on the physical and chemical properties of PA. In addition, two major auto-peaks and one major auto-peak representing C-H functional group are found in synchronous map of the aged PE and PS, respectively (Figs S3 and S4, SI), indicating that the C-H functional group plays a major role in the Cd adsorption process.

3.3 Limitation and further work

The limitation of this study is that the MPs used in this study were virgin commercial plastics, which may be different from the real wastewater-based MPs (Waldman and Rillig 2020). The real MPs entering the WWTPs are affected by a variety of complex factors, such as varying degrees of physical and microbial wear-and-tear in the pipeline network (Bakir et al. 2014, Enfrin et al. 2019). In addition, this study only focuses on the changes in physical and chemical properties of the wastewater-based MP, but it is reported that a large amount of MPs with different weathered characteristics are present in sewage sludge (Li et al. 2020, Mahon et al. 2017, Wei et al. 2019).

However, the effects of sludge treatment on MPs property and their potential risk are still not clearly understood. Therefore, further investigation is needed on the changes in the MPs properties during the real WWTPs and during sludge treatment process in WWTPs such as anaerobic digestion, aerobic composting, dehydration, dewatering and thermal drying.

4. Conclusions

The three wastewater treatment processes cause the MP aging to different degree. Compared to SWPN and MAGT, BTAT has a greater impact on the microscopic features and elemental composition of MPs, due to the attachment of organic matter and microorganisms and the formation of biofilm on the MPs. SWPN and BTAT cause a decrease in zeta potential of the PA, implying an increase in the surface negative charge of PA. Compared with virgin MPs, the adsorption potential of the MPs for Cd decreases after MAGT, but increases after SWPN and BTAT. The treatment processes produce more significant effects on adsorption potential of PS than PE and PA, possibly because other carbon atoms in the PS main chain that are bonded to the benzene ring are more susceptible to chemical attack. Meanwhile, the treatments cause the change in the adsorption mode of the MPs from monolayer to multi-layer. 2D-FTIR COS analysis shows that the N-H functional groups play a great role in the Cd adsorption of the aging PA, while the C-H functional groups are more important for PE and PS. Further investigations need to explore the changes in the MPs properties during the commercial

WWTPs and sludge treatment process in WWTPs.

Acknowledgements

The work was financially supported by National Natural Scientific Foundation of China (52070126), Shanghai Committee of Science and Technology (19DZ1204702), the National Key R&D Program of China (2018YFC1903201), and Program of Shanghai Technology Research Leader Grant (17XD1420500).

Appendix A. Supplementary data

Additional tables and figures as mentioned in the main text. This supporting information is available free of charge via the Internet.

References

Andrady, A.L. (2011) Microplastics in the marine environment. Marine Pollution Bulletin 62(8), 1596-1605.

Babamoradi, H., van den Berg, F., Rinnan, Å. (2013) Bootstrap based confidence limits in principal component analysis – a case study. Chemometrics and Intelligent Laboratory Systems. 120, 97– 105.

Bakir, A., Rowland, S.J. and Thompson, R.C. (2014) Transport of persistent organic pollutants by microplastics in estuarine conditions. Estuarine Coastal and Shelf Science 140, 14-21.

Blair, R.M., Waldron, S. and Gauchotte-Lindsay, C. (2019) Average daily flow of microplastics through a tertiary wastewater treatment plant over a ten-month period. Water Research 163.

Browne, M.A., Niven, S.J., Galloway, T.S., Rowland, S.J. and Thompson, R.C. (2013) Microplastic moves pollutants and additives to worms, reducing functions linked to health and biodiversity. Current Biology 23(23), 2388-2392.

Carr, S.A., Liu, J. and Tesoro, A.G. (2016) Transport and fate of microplastic particles in wastewater treatment plants. Water Research 91, 174-182.
Chen, W., Ouyang, Z.Y., Qian, C. and Yu, H.Q. (2018) Induced structural changes of humic acid by exposure of polystyrene microplastics: A spectroscopic insight. Environmental Pollution 233, 1-7.
Cooper, D.A. and Corcoran, P.L. (2010) Effects of mechanical and chemical processes on the degradation of plastic beach debris on the island of Kauai, Hawaii. Marine Pollution Bulletin 60(5), 650-654.
De Tender, C., Devriese, L.I., Haegeman, A., Maes, S., Vangeyte, J., Cattrijsse, A., Dawyndt, P. and Ruttink, T. (2017) Temporal Dynamics of Bacterial and Fungal Colonization on Plastic Debris in the North Sea. Environmental Science & Technology 51(13), 7350-7360.
Dubaish, F. and Liebezeit, G. (2013) Suspended Microplastics and Black Carbon Particles in the Jade System, Southern North Sea. Water Air and Soil Pollution 224(2).
Edgar, R.C. (2013) UPARSE: highly accurate OTU sequences from microbial amplicon reads. Nature Methods 10(10), 996-+.
Eerkes-Medrano, D., Thompson, R.C. and Aldridge, D.C. (2015) Microplastics in freshwater systems: A review of the emerging threats, identification of knowledge gaps and prioritisation of research needs. Water Research 75, 63-82.
Enfrin, M., Dumee, L.F. and Lee, J. (2019) Nano/microplastics in water and wastewater treatment processes - Origin, impact and potential solutions. Water Research 161, 621-638.
Foo, K.Y. and Hameed, B.H. (2010) Insights into the modeling of adsorption isotherm systems. Chemical Engineering Journal 156(1), 2-10.
Fotopoulou, K.N. and Karapanagioti, H.K. (2012) Surface properties of beached plastic pellets. Marine Environmental Research 81, 70-77.
Fred-Ahmadu, O.H., Bhagwat, G., Oluyoye, I., Benson, N.U., Ayejuyo, O.O. and Palanisami, T. (2020) Interaction of chemical contaminants with microplastics: Principles and perspectives. Science of the Total Environment 706, 135978.
Freeman, S., Booth, A.M., Sabbah, I., Tiller, R., Dierking, J., Klun, K., Rotter, A., Ben-David, E., Javidpour, J. and Angel, D.L. (2020) Between source and sea: The role of wastewater treatment in reducing marine microplastics. Journal Environmental Management 266, 110642.
Fu, D., Zhang, Q., Fan, Z., Qi, H., Wang, Z. and Peng, L. (2019) Aged microplastics polyvinyl chloride interact with copper and cause oxidative stress towards microalgae Chlorella vulgaris. Aquatic Toxicology 216, 105319.
Gewert, B., Plassmann, M.M. and MacLeod, M. (2015) Pathways for degradation of plastic polymers floating in the marine environment. Environmental Science-Processes & Impacts 17(9), 1513-1521.

Guo, X., Hu, G., Fan, X. and Jia, H. (2020) Sorption properties of cadmium on microplastics: The common practice experiment and A two-dimensional correlation spectroscopic study. Ecotoxicology and Environmental Safety 190, 110118.
Guo, X., Pang, J., Chen, S. and Jia, H. (2018) Sorption properties of tylosin on four different microplastics. Chemosphere 209, 240-245.
Holmes, L.A., Turner, A. and Thompson, R.C. (2012) Adsorption of trace metals to plastic resin pellets in the marine environment. Environmental Pollution 160, 42-48.
Holmes, L.A., Turner, A. and Thompson, R.C. (2014) Interactions between trace metals and plastic production pellets under estuarine conditions. Marine Chemistry 167, 25-32.
Iniguez, M.E., Conesa, J.A. and Fullana, A. (2018) Recyclability of four types of plastics exposed to UV irradiation in a marine environment. Waste Management 79, 339-345.
Jin, P.K., Song, J.N., Wang, X.C.C. and Jin, X. (2018) Two-dimensional correlation spectroscopic analysis on the interaction between humic acids and aluminum coagulant. Journal of Environmental Sciences 64, 181-189.
Johansen, M.P., Cresswell, T., Davis, J., Howard, D.L., Howell, N.R. and Prentice, E. (2019) Biofilm-enhanced adsorption of strong and weak cations onto different microplastic sample types: Use of spectroscopy, microscopy and radiotracer methods. Water Research 158, 392-400.
Johansen, M.P., Prentice, E., Cresswell, T. and Howell, N. (2018) Initial data on adsorption of Cs and Sr to the surfaces of microplastics with biofilm. Journal of Environmental Radioactivity 190, 130-133.
Kaiser, D., Kowalski, N. and Waniek, J.J. (2017) Effects of biofouling on the sinking behavior of microplastics. Environmental Research Letters 12(12).
Kelkar, V.P., Rolsky, C.B., Pant, A., Green, M.D., Tongay, S. and Halden, R.U. (2019) Chemical and physical changes of microplastics during sterilization by chlorination. Water Research 163, 114871.
Kent, R.D., Oser, J.G. and Vikesland, P.J. (2014) Controlled evaluation of silver nanoparticle sulfidation in a full-scale wastewater treatment plant. Environmental Science & Technology 48(15), 8564-8572.
Lares, M., Ncibi, M.C., Sillanpaa, M. and Sillanpaa, M. (2018) Occurrence, identification and removal of microplastic particles and fibers in conventional activated sludge process and advanced MBR technology. Water Research 133, 236-246.
Li, S., Liu, H., Gao, R., Abdurahman, A., Dai, J. and Zeng, F. (2018a) Aggregation kinetics of microplastics in aquatic environment: Complex roles of electrolytes, pH, and natural organic matter. Environmental Pollution 237, 126-132.
Li, X., Chen, L., Ji, Y., Li, M., Dong, B., Qian, G., Zhou, J. and Dai, X. (2020) Effects of chemical pretreatments on microplastic extraction in sewage sludge and their physicochemical characteristics. Water Research 171.

Li, X., Chen, L., Mei, Q., Dai, X. and Zeng, E.Y. (2018b) Microplastics in sewage sludge from the wastewater treatment plants in China. Water Research 142, 75-85.
Li, X., Dai, X., Dai, L. and Liu, Z. (2015a) Two-dimensional FTIR correlation spectroscopy reveals chemical changes in dissolved organic matter during the biodrying process of raw sludge and anaerobically digested sludge. RSC Advances 5(100), 82087-82096.
Li, X., Dai, X., Takahashi, J. and Li, N. (2014) New insight into chemical changes of dissolved organic matter during anaerobic digestion of dewatered sewage sludge using EEM-PARAFAC and two-dimensional FTIR correlation spectroscopy. Bioresource Technology 159, 412-420.
Li, X., Dai, X., Yuan, S., Li, N., Liu, Z. and Jin, J. (2015b) Thermal analysis and 454 pyrosequencing to evaluate the performance and mechanisms for deep stabilization and reduction of high-solid anaerobically digested sludge using biodrying process. Bioresource Technology 175, 245-253.
Li, X., Mei, Q., Chen, L., Zhang, H., Dong, B., Dai, X., He, C. and Zhou, J. (2019a) Enhancement in adsorption potential of microplastics in sewage sludge for metal pollutants after the wastewater treatment process. Water Research 157, 228-237.
Li, Y., Li, M., Li, Z., Yang, L. and Liu, X. (2019b) Effects of particle size and solution chemistry on Triclosan sorption on polystyrene microplastic. Chemosphere 231, 308-314.
Liu, P., Qian, L., Wang, H., Zhan, X., Lu, K., Gu, C. and Gao, S. (2019) New Insights into the Aging Behavior of Microplastics Accelerated by Advanced Oxidation Processes. Environmental Science & Technology 53(7), 3579-3588.
Lu, S., Zhu, K., Song, W., Song, G., Chen, D., Hayat, T., Alharbi, N.S., Chen, C. and Sun, Y. (2018) Impact of water chemistry on surface charge and aggregation of polystyrene microspheres suspensions. Science of the Total Environment 630, 951-959.
Mahon, A.M., O'Connell, B., Healy, M.G., O'Connor, I., Officer, R., Nash, R. and Morrison, L. (2017) Microplastics in Sewage Sludge: Effects of Treatment. Environmental Science & Technology 51(2), 810-818.
Mao, R., Lang, M., Yu, X., Wu, R., Yang, X. and Guo, X. (2020) Aging mechanism of microplastics with UV irradiation and its effects on the adsorption of heavy metals. Journal of Hazardous Materials 393, 122515.
McGivney, E., Cederholm, L., Barth, A., Hakkarainen, M., Hamacher-Barth, E., Ogonowski, M. and Gorokhova, E. (2020) Rapid Physicochemical Changes in Microplastic Induced by Biofilm Formation. Frontiers in Bioengineering and Biotechnology 8.
Narancic, T., Verstichel, S., Reddy Chaganti, S., Morales-Gamez, L., Kenny, S.T., De Wilde, B., Babu Padamati, R. and O'Connor, K.E. (2018) Biodegradable Plastic Blends Create New Possibilities for End-of-Life Management of Plastics but They

548 Are Not a Panacea for Plastic Pollution. Environmental Science & Technology
549 52(18), 10441-10452.
550 Rillig, M.C. (2012) Microplastic in Terrestrial Ecosystems and the Soil?
551 Environmental Science & Technology 46(12), 6453-6454.
552 Rom, M., Fabia, J., Grubel, K., Sarna, E., Graczyk, T. and Janicki, J. (2017) Study of
553 the biodegradability of polylactide fibers in wastewater treatment processes. Polimery
554 62(11/12), 834-840.
555 Rummel, C.D., Jahnke, A., Gorokhova, E., Kühnel, D. and Schmitt-Jansen, M. (2017)
556 Impacts of Biofilm Formation on the Fate and Potential Effects of Microplastic in the
557 Aquatic Environment. Environmental Science & Technology Letters 4(7), 258-267.
558 Sintim, H.Y. and Flury, M. (2017) Is Biodegradable Plastic Mulch the Solution to
559 Agriculture's Plastic Problem? Environmental Science & Technology 51(3), 1068-
560 1069.
561 Song, Y.K., Hong, S.H., Jang, M. and Shim, W.J. (2017) Combined Effects of UV
562 Exposure Duration and Mechanical Abrasion on Microplastic Fragmentation by
563 Polymer Type. Environmental Science & Technology 51(8), 4368-4376.
564 Sun, J., Dai, X., Wang, Q., van Loosdrecht, M.C.M. and Ni, B.-J. (2019)
565 Microplastics in wastewater treatment plants: Detection, occurrence and removal.
566 Water Research 152, 21-37.
567 Talvitie, J., Mikola, A., Setala, O., Heinonen, M. and Koistinen, A. (2017) How well
568 is microlitter purified from wastewater? - A detailed study on the stepwise removal of
569 microlitter in a tertiary level wastewater treatment plant. Water Research 109, 164-
570 172.
571 Tampio, E., Ervasti, S., Paavola, T. and Rintala, J. (2016) Use of laboratory anaerobic
572 digesters to simulate the increase of treatment rate in full-scale high nitrogen content
573 sewage sludge and co-digestion biogas plants. Bioresource Technology 220, 47-54.
574 Tang, C.Y.Y., Kwon, Y.N. and Leckie, J.O. (2009) Effect of membrane chemistry and
575 coating layer on physiochemical properties of thin film composite polyamide RO and
576 NF membranes I. FTIR and XPS characterization of polyamide and coating layer
577 chemistry. Desalination 242(1-3), 149-167.
578 Ter Halle, A., Ladirat, L., Gendre, X., Goudouneche, D., Pusineri, C., Routaboul, C.,
579 Tenailleau, C., Duployer, B. and Perez, E. (2016) Understanding the Fragmentation
580 Pattern of Marine Plastic Debris. Environmental Science & Technology 50(11), 5668-
581 5675.
582 Tribedi, P. and Sil, A.K. (2013) Low-density polyethylene degradation by
583 Pseudomonas sp AKS2 biofilm. Environmental Science and Pollution Research 20(6),
584 4146-4153.
585 Turner, A. and Holmes, L.A. (2015) Adsorption of trace metals by microplastic pellets
586 in fresh water. Environmental Chemistry 12(5), 600-610.
587 Van Cauwenberghe, L., Vanreusel, A., Mees, J. and Janssen, C.R. (2013) Microplastic
588 pollution in deep-sea sediments. Environmental Pollution 182, 495-499.

589 Waldman, W.R. and Rillig, M.C. (2020) Microplastic Research Should Embrace the
590 Complexity of Secondary Particles. Environmental Science & Technology 54(13),
591 7751-7753.
592 Wang, F., Wong, C.S., Chen, D., Lu, X., Wang, F. and Zeng, E.Y. (2018) Interaction of
593 toxic chemicals with microplastics: A critical review. Water Research 139, 208-219.
594 Wang, J., Tan, Z., Peng, J., Qiu, Q. and Li, M. (2016) The behaviors of microplastics
595 in the marine environment. Marine Environmental Research 113, 7-17.
596 Wei, W., Zhang, Y.-T., Huang, Q.-S. and Ni, B.-J. (2019) Polyethylene terephthalate
597 microplastics affect hydrogen production from alkaline anaerobic fermentation of
598 waste activated sludge through altering viability and activity of anaerobic
599 microorganisms. Water Research 163.
600 Wijesekara, H., Bolan, N.S., Bradney, L., Obadamudalige, N., Seshadri, B.,
601 Kunhikrishnan, A., Dharmarajan, R., Ok, Y.S., Rinklebe, J., Kirkham, M.B. and
602 Vithanage, M. (2018) Trace element dynamics of biosolids-derived microbeads.
603 Chemosphere 199, 331-339.
604 Wu, X., Liu, P., Huang, H. and Gao, S. (2020) Adsorption of triclosan onto different
605 aged polypropylene microplastics: Critical effect of cations. Science of the Total
606 Environment 717, 137033.
607 Xu, B., Liu, F., Brookes, P.C. and Xu, J. (2018) Microplastics play a minor role in
608 tetracycline sorption in the presence of dissolved organic matter. Environmental
609 Pollution 240, 87-94.
610 Yang, A.J. (1998) statistical mechanical study on the freundlich isotherm equation.
611 Journal of Colloid and Interface Science 208 (2), 379-387.
612 Zettler, E.R., Mincer, T.J. and Amaral-Zettler, L.A. (2013) Life in the "Plastisphere":
613 Microbial Communities on Plastic Marine Debris. Environmental Science &
614 Technology 47(13), 7137-7146.
615 Zhang, H., Wang, J., Zhou, B., Zhou, Y., Dai, Z., Zhou, Q., Chriestie, P. and Luo, Y.
616 (2018) Enhanced adsorption of oxytetracycline to weathered microplastic
617 polystyrene: Kinetics, isotherms and influencing factors. Environmental Pollution
618 243, 1550-1557.
619 Zhang, X., Chen, J. and Li, J. (2020) The removal of microplastics in the wastewater
620 treatment process and their potential impact on anaerobic digestion due to pollutants
621 association. Chemosphere 251, 126360.
622 Zou, J., Liu, X., Zhang, D. and Yuan, X. (2020) Adsorption of three bivalent metals
623 by four chemical distinct microplastics. Chemosphere 248, 126064.
624 Zubris, K.A. and Richards, B.K. (2005) Synthetic fibers as an indicator of land
625 application of sludge. Environmental pollution (Barking, Essex : 1987) 138(2), 201-
626 211.
627
628

629 Table 1. Elemental composition of the virgin and treated MPs

Samples`	C	H	N	S	O	Elemental ratio	
	(%)	(%)	(%)	(%)	(%)	C/H	O/C
Virgin PA	64.30±0.30	9.60	13.00	ND [d]	13.10	0.56	0.15
SWPN[a] PA	62.95±1.00	9.51±0.20	11.93±0.10	ND	15.61	0.56	0.19
MAGT [b] PA	62.19	9.21	10.99	ND	17.61	0.57	0.21
BTAT [c] PA	56.33±0.50	8.54±0.20	10.83±0.06	0.30±0.22	24.00	0.55	0.32
Virgin PE	86.32±0.80	13.66±0.10	0.02±0.01	ND	ND	0.53	ND
SWPN PE	85.25±1.80	13.60±0.30	0.02±0.01	ND	1.14	0.52	0.01
MAGT PE	82.55	13.42	0.04	ND	4.00	0.51	0.04
BTAT PE	73.14	11.89	0.32	ND	14.65	0.51	0.15
Virgin PS	92.36±0.70	7.64±0.04	ND	ND	ND	1.01	ND
SWPN PS	91.89 ±1.70	7.61±0.14	ND	ND	0.50	1.01	0.004
MAGT PS	91.20	7.91	0.00	ND	0.89	0.96	0.007
BTAT PS	69.09±0.18	6.10±0.03	0.68±0.18	0.05±0.01	24.08	0.94	0.26

630 [a], SWPN, sulfidation in wastewater pipeline network; [b], MAGT, mechanical abrasion in grit tank; [c],

631 BTAT, biological treatment in aeration tank; [d] ,not detectable

632 Table 2. Zeta potential of the virgin and treated MPs

MP samples	PA	PE	PS
Virgin MP	0.55±0.01	-2.02±0.32	-2.04±0.44
SWPN MP [a]	-0.16±0.24	-1.13±0.11	-2.16±0.66
MAGT MP [b]	0.95±0.45	-3.26±0.51	-2.82±0.86
BTAT MP [c]	-0.57±0.52	-2.48±0.22	-3.04±0.58

633 [a], SWPN, sulfidation in wastewater pipeline network; [b], MAGT, mechanical abrasion in grit tank; [c],

634 BTAT, biological treatment in aeration tank

635 Table 3. Adsorption isotherm constants defining Cd adsorption on the virgin and treated MPs

636 according to the isotherm model.

MP samples	Langmuir isotherm	Freundlich isotherm
Virgin PA	k_L=0.320 L μg^{-1}	k_F=5.28 μg$^{1-1/n}$ g^{-1} L$^{1/n}$
	q_{max}=0.3396 mg g^{-1}	n=2.58
	R^2=0.89	R^2=0.83
SWPN[a] PA	k_L=0.53 L μg^{-1}	k_F=102.35 μg$^{1-1/n}$ g^{-1} L$^{1/n}$
	q_{max}=2.13 mg g^{-1}	n=13.35
	R^2=0.97	R^2=0.80
MAGT[b] PA	k_L=6.27 L μg^{-1}	k_F=1.79 μg$^{1-1/n}$ g^{-1} L$^{1/n}$
	q_{max}=25.74 μg g^{-1}	n=2.07
	R^2=0.63	R^2=0.87
BTAT[c] PA	k_L=4.588 L μg^{-1}	k_F=9.67 μg$^{1-1/n}$ g^{-1} L$^{1/n}$
	q_{max}=543.5 μg g^{-1}	n=1.98
	R^2=0.70	R^2=0.92
Virgin PE	k_L=0.414 L μg^{-1}	k_F=4.53 μg$^{1-1/n}$ g^{-1} L$^{1/n}$
	q_{max}=0.2345μg g^{-1}	n=3.7
	R^2=0.92	R^2=0.89
SWPN PE	k_L=8.80 L μg^{-1}	k_F=10.41 μg$^{1-1/n}$ g^{-1} L$^{1/n}$
	q_{max}=360.9 μg g^{-1}	n=2.4
	R^2=0.75	R^2=0.99
MAGT PE	k_L=7.97 L μg^{-1}	k_F=6.68 μg$^{1-1/n}$ g^{-1} L$^{1/n}$
	q_{max}=126.5 μg g^{-1}	n=10.50
	R^2=0.97	R^2=0.24
BTAT PE	k_L=0.745 L μg^{-1}	k_F=20.03 μg$^{1-1/n}$ g^{-1}L$^{1/n}$
	q_{max}=614.48 μg g^{-1}	n=5.01
	R^2=0.87	R^2=0.45
Virgin PS	k_L=0.516L μg^{-1}	k_F=1.11 μg$^{1-1/n}$ g^{-1}L$^{1/n}$
	q_{max}=0.0699 μg g^{-1}	n=2.23
	R^2=0.81	R^2=0.66
SWPN PS	k_L=3.062 L μg^{-1}	k_F=7.20 μg$^{1-1/n}$ g^{-1} L$^{1/n}$
	q_{max}=34.64 μg g^{-1}	n=1.83
	R^2=0.62	R^2=0.97
MAGT PS	k_L=31.81 L μg^{-1}	k_F=3.25 μg$^{1-1/n}$ g^{-1} L$^{1/n}$

	q_{max}=57.48 μg g^{-1}	n=5.43
	R^2=0.97	R^2=0.45
BTAT PS	k_L=0.798 L $μg^{-1}$	k_F=15.05 $μg^{1-1/n}$ g^{-1} $L^{1/n}$
	q_{max}=1029.3 μg g^{-1}	n=2.43
	R^2=0.80	R^2=0.89

637 [a], SWPN, sulfidation in wastewater pipeline network; [b], MAGT, mechanical abrasion in grit tank; [c],

638 BTAT, biological treatment in aeration tank

Figure Caption

Fig. 1. Scanning electron micrograph of virgin and treated MPs. SWPN, sulfidation in wastewater pipeline network; MAGT, mechanical abrasion in grit tank; BTAT, biological treatment in aeration tank

Fig. 2. Microbial community composition in activated sludge from aeration tank after the addition of the MPs for 14 days at genus level

Fig. 3. Changes in adsorption potentials of virgin and treated MPs to Cd. SWPN, sulfidation in wastewater pipeline network; MAGT, mechanical abrasion in grit tank; BTAT, biological treatment in aeration tank

Fig. 4. Adsorption isotherms of virgin and treated MPs to Cd. SWPN, sulfidation in wastewater pipeline network; MAGT, mechanical abrasion in grit tank; BTAT, biological treatment in aeration tank

Fig. 5. Synchronous (left) and asynchronous (right) 2D correlation maps generated from the 700–1700 cm^{-1} region of the FTIR spectra of treated PA samples with the Cd adsorption. a, sulfidation in wastewater pipeline network (SWPN); b, mechanical abrasion in grit tank (MAGT); c, biological treatment in aeration tank (BTAT).

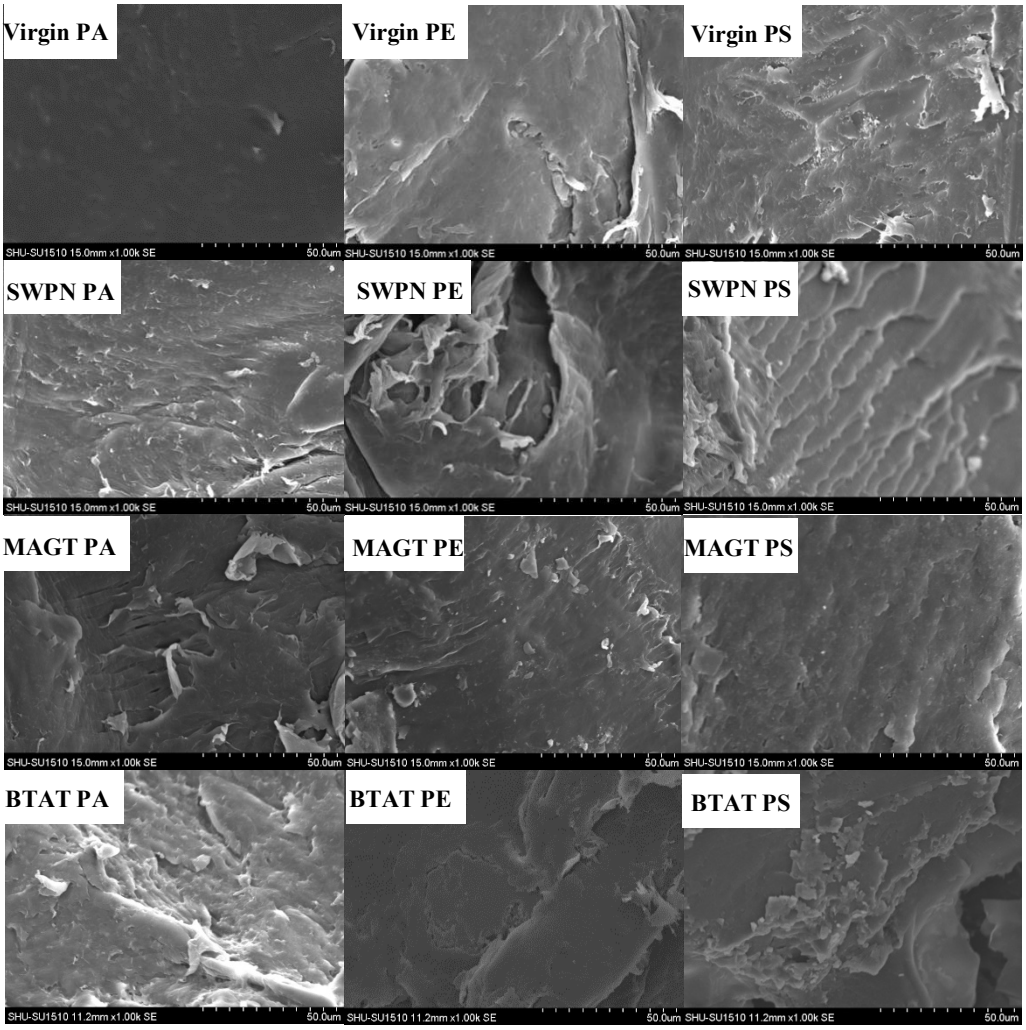

655 Fig. 1. SEM of virgin and treated MPs. SWPN, sulfidation in wastewater pipeline network; MAGT,

656 mechanical abrasion in grit tank; BTAT, biological treatment in aeration tank

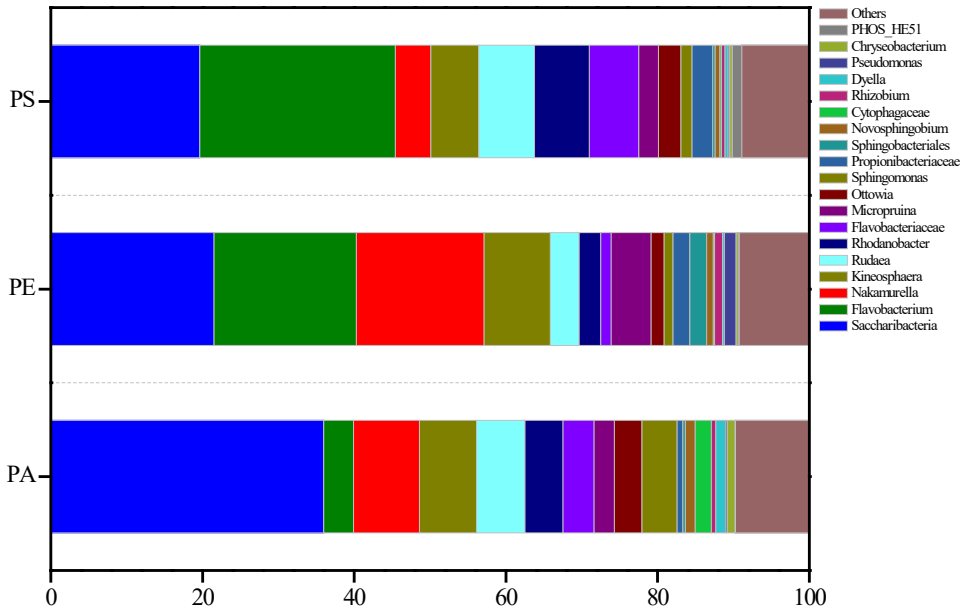

657

658 Fig. 2. Microbial community composition at genus level in activated sludge from aeration tank after

659 the addition of the MPs for 14 days

660

661

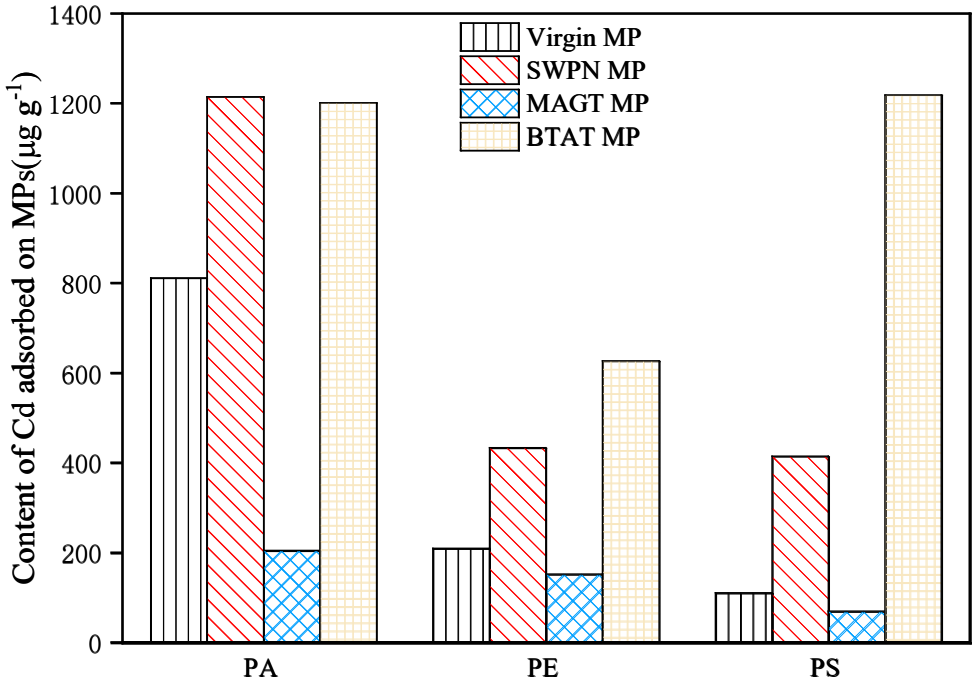

662

663 Fig. 3. Changes in adsorption potentials of virgin and treated MPs for Cd. SWPN, sulfidation in

664 wastewater pipeline network; MAGT, mechanical abrasion in grit tank; BTAT, biological treatment

665 in aeration tank

666

667

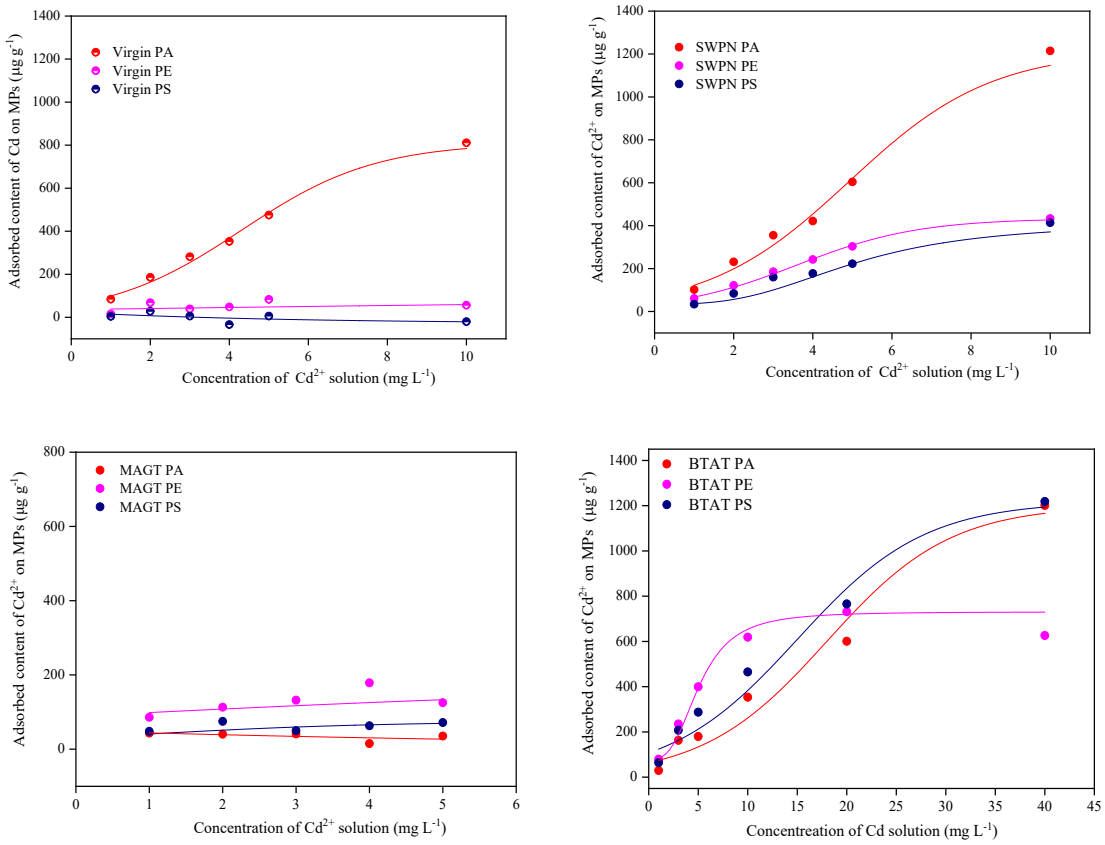

668

669 Fig. 4. Adsorption isotherms of virgin and treated MPs for Cd. SWPN, sulfidation in wastewater

670 pipeline network; MAGT, mechanical abrasion in grit tank; BTAT, biological treatment in aeration

671 tank

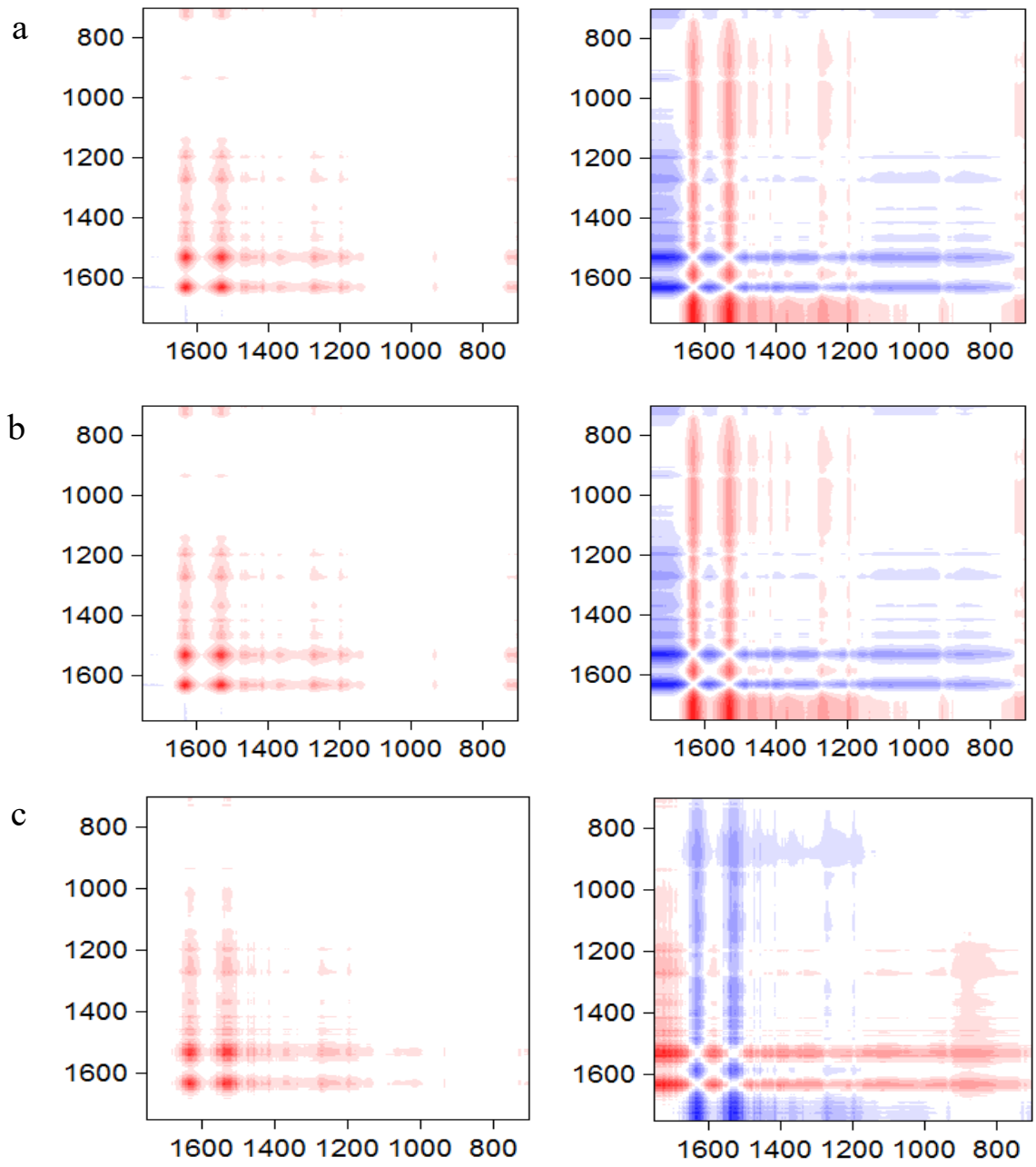

Fig. 5. Synchronous (left) and asynchronous (right) 2D correlation maps generated from the 700–1700 cm^{-1} region of the FTIR spectra of treated PA samples with the Cd adsorption. a, sulfidation in wastewater pipeline network; b, mechanical abrasion in grit tank; c, biological treatment in aeration tank.